

# Numerical Simulations of an X-Band Antenna-Amplifier Device<sup>1</sup>

A.S. Shlapakovski, W. Jiang\*, and E. Schamiloglu\*\*

*Nuclear Physics Institute, 2a Lenina Str., Tomsk, 634050, Russia  
Phone: 7-382-241-7959, Fax: 7-382-242-3934, E-mail: shl@npi.tpu.ru  
\* Nagaoka University of Technology, Nagaoka, Niigata 940-2188, Japan  
\*\* University of New Mexico, Albuquerque NM, 87131, USA*

**Abstract – The results of particle-in-cell simulations of annular electron beam interaction with the non-axisymmetric HE<sub>11</sub> mode in the antenna-amplifier device using the 3-D version of the MAGIC code are presented. The results have been obtained for the real geometry and parameters of electron diode and interaction space to be used in the experiments planned to prove the antenna-amplifier concept; these parameters provide the operating HE<sub>11</sub> mode being dominant. Achievable gain, bandwidth, and device efficiency have been investigated at different values of the interaction region length, input RF power and pulse duration. The peak gain occurs at a 9.3 GHz drive frequency, it reaches ~18.5 dB with the interaction space length of ~25 cm. At the increased interaction region length and RF drive power, the device efficiency reaches ~15% at an output power of ~30 MW. Simulations with the short RF drive pulse have also been carried out.**

## 1. Introduction

An antenna-amplifier, Cherenkov maser with a rod slow-wave structure operating in the non-axisymmetric HE<sub>11</sub> mode (fundamental mode of a dielectric rod antenna), can be a compact, controllable, high-power microwave source [1]. The first antenna-amplifier simulation results obtained using the 3-D version of the MAGIC particle-in-cell code were presented in our earlier work [2]. Those initial simulations were performed for an idealized geometry and simplified model of particles emission not accounting for the conditions of electron beam generation in a real diode configuration. Also, the parameters taken for simulations in [2] corresponded to the physical situation allowing for the RF drive frequency harmonics generation due to excitation of higher-order modes at the nonlinear stage of interaction, and the goal was to verify possibilities of novel tuning schemes for controlling harmonics content in the output signal spectrum.

Meanwhile, the proof-of-principle experiments are planned [3] on gain demonstration in the X-band antenna-amplifier. Parameters chosen for these experi-

ments correspond to the situation of the operating HE<sub>11</sub> mode being dominant, and the annular electron beam is produced from the explosive emission cathode of the magnetically insulated diode. The objective of the present work is to investigate achievable gain and bandwidth for the geometry close to that of the proof-of-principle experiments and current model experiments on beam transport [3]. Also important is to study the electric field produced along the dielectric surface inside the annular beam.

## 2. Simulations for the coaxial diode geometry

The coaxial diode geometry corresponds to the case of already performed model experiments on beam generation and transport in the guide magnetic field without the RF drive signal [3]. The configuration of the simulation space is presented in Fig. 1.

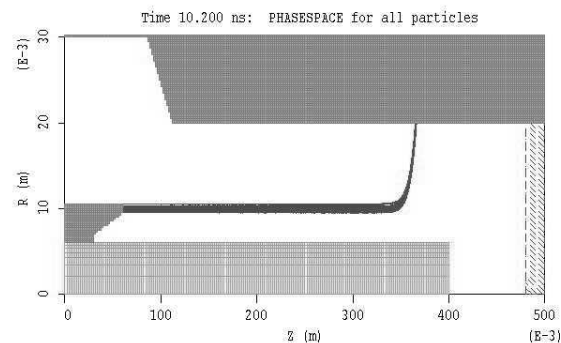


Fig. 1. System geometry and beam axial cross-section

The boundary in radial direction is formed by the conducting anode (3 cm radius) and drift tube (2 cm radius) with the tapered buffer section of 26 mm length in between. Inside the conducting cathode, the dielectric rod (6 mm radius,  $\epsilon = 5$ ) is inserted. At the left boundary, two ports are set: outer (with respect to the cathode) for the voltage applied, and inner for the microwave input. The right boundary was set as FREESPACE. The EMISSION EXPLOSIVE command was used to set particles emission. The emitting edge of the cathode is of 1 mm thickness and 10 mm mean radius; its axial coordinate was 6 cm in all simulations. Tapered region inside the cathode is the same

<sup>1</sup> The work was supported in part by Russian Foundation for Basic Research (grant no. 05-08-01150) and Asian Office of Aerospace Research and Development (AOARD-05-4041).

as used in the experiments; the rest of cathode geometry is simplified. The input voltage set at the left boundary was adjusted in the way providing the diode voltage of  $\sim 290$  kV and beam current of  $\sim 1.17$  kA. The beam was guided by a strong preset magnetic field (3.0 T), so that the length of this preset field determined the interaction region length. The input X-band signal was injected in the fundamental  $TE_{11}$  mode of the waveguide totally filled with the dielectric, which excited (being very similar in field pattern) the  $HE_{11}$  mode of the dielectric rod. The signal was linearly polarized, i.e., the  $TE_{11}$  mode field pattern was fixed in time keeping purely radial electric component along the horizontal line (azimuth  $\varphi = 0$ ). Typical run time for simulations was 10.2 ns.

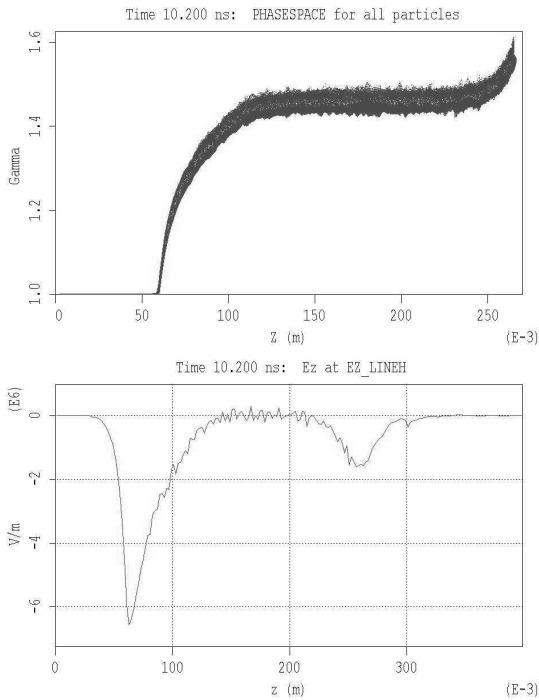


Fig. 2. Electrons Lorentz factor (top) and  $E_z$  field at the rod radius vs.  $z$  coordinate (bottom). No RF input

For the case of no RF signal at the input, the simulations were performed at the magnetic field length (and entire simulation space) 10 cm shorter than shown in Fig. 1. The beam phase portrait and axial electric field at the rod surface (inside the beam) are presented in Fig. 2. It is seen from the phase space plot that at the acceleration stage, the beam acquires a significant energy spread determined both by its finite thickness and explosive emission process. As to the electric field under the beam, it is practically absent in the region of phase space uniformity, since the dc space charge field inside a uniform annular beam is zero.  $E_z$  is non-zero in the region of acceleration and beam dump, and its actual values are important as this field may cause the surface breakdown along the rod. At the beam dump,  $E_z \sim 15$ -16 kV/cm, that seems quite acceptable. Its maximum value falls to  $\sim 3$  mm

downstream of the cathode edge location and exceeds 60 kV/cm; this implies a certain requirements on the rod material electric strength and vacuum conditions.

The radiation downstream of the beam dump produced in case of no RF input signal represents the beam noise. There is the peak of  $\sim 60$  kW in the power time dependence corresponding to the moment of the beam head reaches the dump place. After that, the power falls down to several kilowatts. The spectrum is noisy with the maximum at the X-band as expected.

### 3. RF at the input: linear stage

For the results obtained with the RF drive signal at the inner input port, which are presented in this section, the lengths of beam, rod, and entire simulation space were exactly as shown in Fig. 1. Simulations performed at different drive frequencies have shown the maximum gain at 9.3 GHz. The beam bunching in the non-axisymmetric RF field is clearly expressed as seen from the top plot of Fig. 3. The gain is seen from two other plots of Fig. 3 showing the input and output RF power time dependences at this frequency.

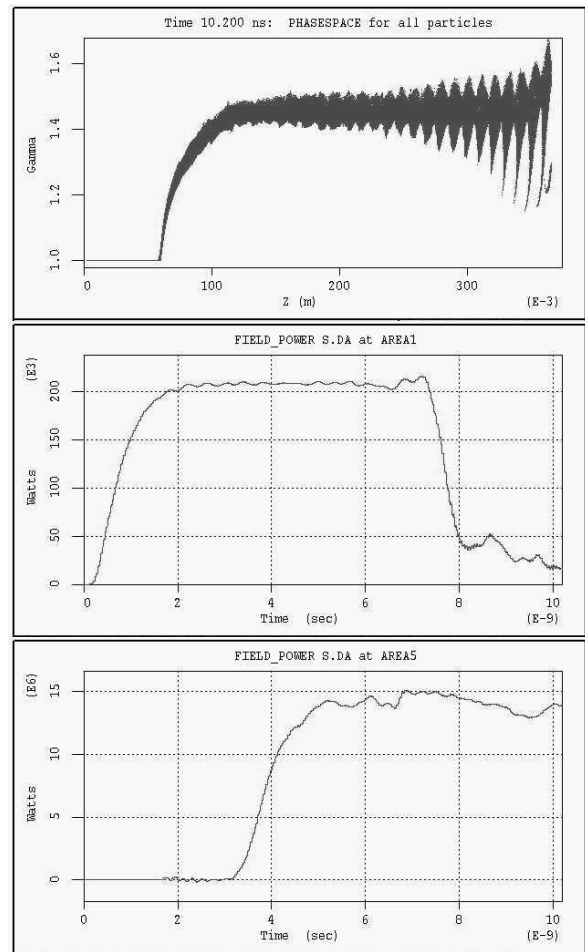


Fig. 3. Beam phase portrait and RF powers observed at 1 cm from the input port (middle) and 1 cm before the rod end (bottom) for 9.3 GHz drive frequency

The input power is obtained by integrating Poynting flux over the inner waveguide cross-section. The decrease in the observed power near the input appears due to reflection from the rod end. It should be noted that simulations were carried out with the rod tapering at its end as well; this eliminates reflection but weakly affects the gain. The output power is obtained by integrating Poynting flux over the drift tube cross-section downstream of the beam dump but still including dielectric, upstream of its end, because in the real antenna-amplifier geometry, dielectric extends out of vacuum space. Thus, comparing the output power in Fig. 3 (13-15 MW) to the input power (~210 kW), one can conclude that the maximum gain at the given beam length reaches ~18.5 dB.

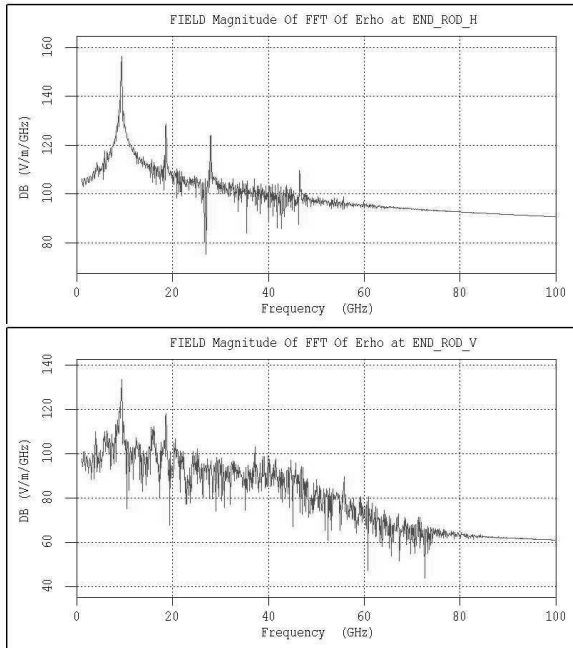


Fig. 4. Output spectrum (9.3 GHz RF input). The observation points are at the rod radius, 1 cm before its end, at azimuths  $\varphi = 0$  (top) and  $\varphi = 90^\circ$  (bottom)

The radiation spectrum at the output is presented in Fig. 4 as the FFT of the radial electric field time behavior for two points of different azimuthal positions: one corresponding to the input wave polarization and another one, at which the input wave has zero  $E_r$  component. It is seen that the peak corresponding to the drive frequency is much higher at the top plot; also, the rest of spectrum at  $\varphi = 90^\circ$  is noisy whereas at  $\varphi = 0$ , frequency harmonics are clearly expressed. Evidently, the peak at the drive frequency in the point where the  $HE_{11}$  mode has zero  $E_z$  component is associated with non-synchronous ac space charge oscillations. This is well seen from the comparison of the plots showing  $E_z$  component profiles along the rod for these two azimuths, which are given in Fig. 5. The field profile at  $\varphi = 90^\circ$  is similar to that obtained without RF input (Fig. 2), whereas the profile at  $\varphi = 0$

associated with the amplified RF signal is extremely different. This field is even higher than the field under the cathode edge; to eliminate a breakdown along the rod at the device output, the RF drive pulse should be short enough.

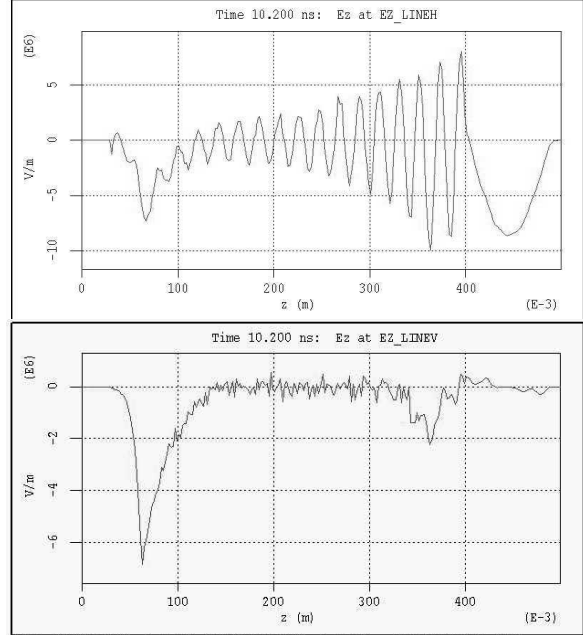


Fig. 5.  $E_z$  field instantaneous profiles at the rod surface for  $\varphi = 0$  (top) and  $\varphi = 90^\circ$  at 9.3 GHz RF input

The amplification band obtained in the simulations coincides with the tuning range of the magnetron to be employed for RF drive pulse generation in the planned experiments. Both gain and bandwidth computed using MAGIC are in the good agreement with the results obtained from the solution of the linear theory dispersion relation. In particular, some bandwidth asymmetry was observed, e.g., the simulation at the frequency of 10.0 GHz exhibited, in fact, neither bunching, no gain, whereas at the lower frequency of 8.6 GHz, which is symmetrically distanced from the peak gain frequency, the gain and bunching were still observed. The gain in this case was as low as ~11 dB.

#### 4. Nonlinear regime: increased length and RF drive power

At the increased length of the interaction region and higher RF power at the input port, the simulated amplifier exhibits deviation from linearity, both in the output vs. input power dependence and in the gain per unit length. In Fig. 6, the results are presented for the simulations performed at the guide magnetic field, dielectric rod, and entire simulation space 5 cm longer compared to those of the previous section. It is seen from the top plot that in case of the same input power and frequency as in the previous section, the output power reaches 24-25 MW. That means the output power increase (compared to 13-15 MW of the bottom plot of Fig. 3) is much less than ~5 dB, the value one

could get from the linear gain of  $\sim 1$  dB/cm. Nonlinear effects are clearly manifested in the middle plot of Fig. 6 showing the beam bunching and obvious from the comparison of the output powers observed at different drive powers (top and bottom plots).

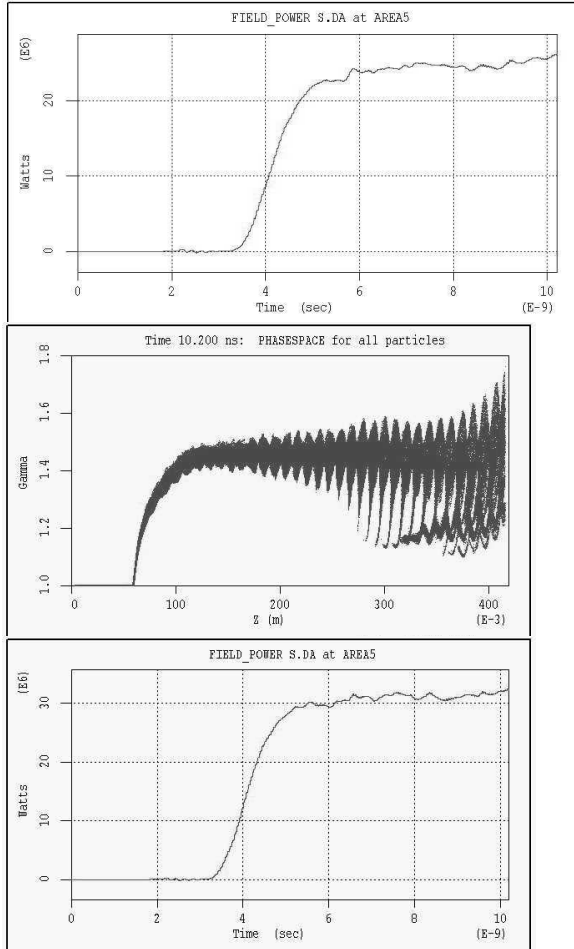


Fig. 6. Simulations for the interaction region length increased by 5 cm (9.3 GHz drive frequency). Output power at 1 cm before the rod end for  $\sim 210$  kW input power (top), beam phase portrait and output power for  $\sim 535$  kW input power (middle and bottom).

Finally, it is seen that one can reach the efficiency of  $\sim 15\%$  at  $\sim 30$  MW output power level. It should be noted also that the harmonics level in case of maximum output power does not increase.

**5. Quasiplanar diode geometry and finite RF drive pulse length**

For the proof-of-principle experiments [3], the diode geometry will rather be modified in order to have the possibility of the beam current variation at a given diode voltage. In this, in fact, quasiplanar geometry, the cathode edge is located much closer to the drift tube entrance, and the anode diameter is large enough, so that it weakly affects the diode impedance. Also, with the quasiplanar geometry (it is shown in Fig. 7),

the region of beam acceleration shortens that can result in a higher gain as this region is, at least, useless for the Cherenkov interaction with the input RF wave.

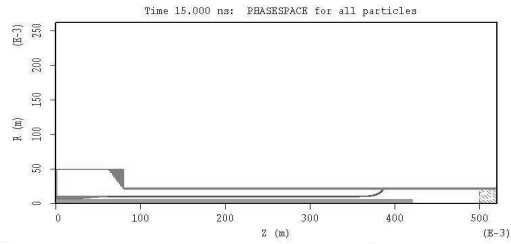


Fig. 7. Simulation space in case of quasiplanar diode.

Also significant is that for the proof-of-principle experiments, the RF drive pulse is planned to be much shorter than the beam pulse [3]. We simulated this situation by setting the finite duration of the input signal and increasing the run time up to 15 ns as is seen in Fig. 8. The negative power in the top plot is due to the reflection from the rod end. The reflection back from the cathode results in  $\sim 1.6$  MW post-radiated power that appears at the output cross-section after the main pulse of 20-22 MW (bottom plot).

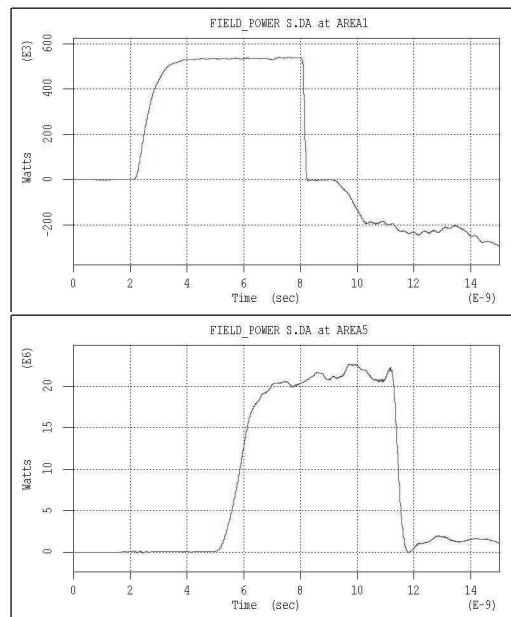


Fig. 8. RF input (1 cm from the input port, top) and output (1 cm before the rod end, bottom) powers for 9.3 GHz drive frequency and geometry of Fig. 7. Diode voltage is  $\sim 270$  kV, beam current is  $\sim 1.07$  kA.

**References**

[1] A.S.Shlapakovski, I.I.Vintzenko, A.V.Petrov, and E.Schamiloglu, in *Proc. 13<sup>th</sup> Symposium on High-Current Electronics*, 2004, pp. 224-227.  
 [2] A.Shlapakovski, W.Jiang, E.Schamiloglu, in *Proc. 14<sup>th</sup> Int. Pulsed Power Conf.* 2003, pp. 1169-1172.  
 [3] A.S.Shlapakovski, S.N.Artemenko, et al., in *Proc. 14<sup>th</sup> Symposium on High-Current Electronics*, 2006 (this issue).